Optical Materials 92 (2019) 30–35

Contents lists available at ScienceDirect

Optical Materials

journal homepage: www.elsevier.com/locate/optmat

Enhanced bremsstrahlung X-ray emission from Ag nanoparticles irradiated by ultrashort laser pulses

Pranitha Sankar[a,b], Jyothis Thomas[a], H.D. Shashikala[b], Reji Philip[a,*]

[a] Ultrafast and Nonlinear Optics Lab, Light and Matter Physics Group, Raman Research Institute, Bangalore, 560080, India
[b] Department of Physics, National Institute of Technology Karnataka, Surathkal, India

ARTICLE INFO

Keywords:
Laser produced plasma
X-ray emission
Metal nanoparticle
Bremsstrahlung emission

ABSTRACT

In this work, an Ag nanoparticle colloidal suspension flowing in the form of a thin jet (250 μm) is irradiated by 150 femtosecond, 800 nm laser pulses to form a plasma which emits bremsstrahlung X-rays of up to 100 keV energy. The flowing jet ensures long-term durability of the plasma source during continuous laser irradiation. The laser pulse is p-polarized and the angle of incidence is normal to the jet surface, to optimize resonance absorption of laser radiation by the plasma electron density gradient. A 30-fold enhancement is observed in the X-ray yield in the nanoparticle suspension, compared to the precursor salt solution. This is because of the local field enhancement (LFE) associated with the localized surface plasmon resonance (LSPR) in Ag nanoparticles. Multiphoton ionization will be greatly enhanced in the presence of LFE, resulting in the generation of a relatively larger number of free electrons, which become "hot" electrons of high kinetic energy by resonance absorption. Bremsstrahlung in the X-ray regime occurs due to the deceleration of these hot electrons. Under identical excitation conditions the corresponding X-ray enhancement measured in Au nanoparticles is relatively lower at 18-fold. This decrease is due to the higher ionization potential of Au (9.22 eV) as compared to Ag (7.58 eV). On the other hand, absorption spectra and SEM images measured after continuous irradiation reveal that Au nanoparticles are more photostable compared to Ag nanoparticles. These studies show that Ag nanoparticles are better suited for X-ray generation compared to Au nanoparticles under the experimental conditions employed. Applications include dynamics studies, microscopy, and lithography.

1. Introduction

Research efforts are currently underway to optimize plasma X-ray sources produced by ultrashort laser pulses, which will be useful for X-ray lasing [1] and soft X-ray microscopy [2], and for probing ultrafast real-time physical, chemical and biological dynamics [3,4]. Dense plasmas produced by intense ultrashort laser pulses open up additional possibilities like table top acceleration [5] and synchrotron radiation [6]. Solid targets such as metals [7] and transparent glasses [8] have been used for X-ray generation under intense femtosecond laser irradiation, while compact and efficient soft and hard X-ray sources have been developed from porous and nanocylinder [9] targets, and from structured surfaces such as gratings [10,11] and "velvet" coatings [12]. There is a great deal of interest in techniques which can enhance the X-ray yield, and the effects of various laser parameters and targets have been the subject of a few studies [13,14]. Among different materials, metal nanoparticles and carbon allotropes have received particular attention for generating ultrashort electron bunches with proven ability to generate X-rays [13,14,15,16].

The advantage of using metal nanoparticles for generating X-rays primarily stems from the local field enhancement (LFE) in them, which is associated with the localized surface plasmon resonance (LSPR). LFE results in enhanced multiphoton ionization (MPI) because an nth order multiphoton process scales in magnitude as I^n, where I is the optical intensity. MPI generates free electrons which become "hot" electrons with high kinetic energy by resonance absorption of photons from the laser pulse. When these hot electrons decelerate, bremsstrahlung emission of X-rays occurs. Increase in X-ray flux can therefore be achieved by increasing the number (not necessarily temperature though temperature increase can be beneficial) of hot electrons which are the primary drivers for Bremsstrahlung. This amounts to finding schemes to generate more electrons per photon delivered into the plasma. In addition to employing LFE, the target also can be chosen appropriately. In this paper we explore a combined scheme wherein the use of noble metal nanoparticles achieves the former, while the choice of lower ionization potential (Ag instead of Au) achieves the latter.

* Corresponding author.
E-mail address: reji@rri.res.in (R. Philip).

https://doi.org/10.1016/j.optmat.2019.03.055
Received 31 January 2019; Received in revised form 12 March 2019; Accepted 29 March 2019
Available online 12 April 2019
0925-3467/

Liquid targets are increasingly being considered nowadays as laser plasma X-ray sources because emission can be controlled by a proper selection of the solute in solution or suspension. Moreover, liquids can be continuously circulated using a small pump, to make them durable for long-term laser irradiation and X-ray generation. Regardless, little attention has been paid into improving the yield of hard X-rays (> 10 keV) from liquid targets. In the present work we report features of hard X-ray emission from a laser induced plasma of Ag nanoparticles of 20 nm mean size, dispersed in water and circulated through a flat, thin (250 μm) metal nozzle to form a jet stream. The jet is irradiated by 800 nm ultrashort laser pulses of 150 fs pulsewidth (FWHM). For comparative purposes we run the same experiments for Au nanoparticles, and the results show that X-ray emission from Ag nanoparticles is brighter in comparison.

2. Materials and methods

Silver nanoparticles were synthesized by employing sodium borohydride (NaBH4) as reductant [17]. A typical procedure is as follows. Required volumes of freshly prepared aqueous solutions containing $AgNO_3$ and TSC are mixed and heated to 60 °C for 30 min in the dark with vigorous stirring to ensure a homogenous solution. At the end of 30 min the required volume of $NaBH_4$ solution is added drop-wise to the mixture, and subsequently, the temperature is further raised to 90 °C. Heating is continued for 5 min, until a change of colour is evident. The nanoparticle suspension is allowed to cool at room temperature and is finally stored at 4 °C for future use. The concentration of the nanoparticles is estimated to be $2.45 \times 10^{15}\,cm^{-3}$. In this method sodium borohydride ($NaBH_4$) is used for reducing Ag atoms which would form the nanoparticle nuclei. Overall the process is similar to reduction using citrate but sodium borohydride provides better monodispersity for the final particle population because $NaBH_4$ is a stronger reducing agent compared to citrate.

Au nanoparticles were prepared by the Turkevich Method [18], as outlined by Wei-Hung Hsu et al. [14]. In this method, Au nanoparticles are produced in a liquid by the reduction of hydrogen tetrachloroaurate (III) trihydrate ($H[AuCl_4]$). After dissolving $H[AuCl_4]$ the solution is heated to boiling and rapidly stirred while the reducing agent (sodium citrate) is added. This causes Au^{3+} ions to be reduced to Au^{+} ions. Then a disproportionation reaction occurs whereby $3Au^{+}$ ions give rise to Au^{3+} and $2Au^{0}$ atoms. The Au^{0} atoms act as centres of nucleation around which further Au^{+} ions get reduced. To prevent the particles from aggregating, a stabilizing agent that sticks to the nanoparticle surface is required. Here, citrate initially acts as the reducing agent and finally as the capping agent, which stabilizes the Au nanoparticles through electrostatic interactions between the lone pair of electrons on the oxygen and the metal surface.

Linear absorption spectra of the prepared nanoparticle solutions (measured using an Agilent Cary 5000 double-beam spectrophotometer with a resolution of 2 nm) are shown in Fig. 1a. For measuring these spectra the samples were taken in 5 mm path length cuvettes. Absorption bands arising from LSPR can be seen in the region of 380–480 nm for Ag nanoparticles, and 520–600 nm for Au nanoparticles. From SEM images taken using thin films of the solutions on ITO sheets it can be seen that the as prepared nanoparticles are not aggregated in solution. Size distribution histograms for the nanoparticles were calculated from SEM images using the ImageJ software. The mean size of Ag and Au nanoparticles are found to be 20 ± 2 nm and 21 ± 3 nm respectively.

The schematic of the experimental setup is shown in Fig. 2. 250 ml volume of the liquid sample is taken in a source beaker, which is driven into a drain beaker through a flat, narrow metal nozzle using a small pump. Flow through the nozzle provides a thin planar jet (250 μm thickness) of the liquid. The jets are irradiated normal to the surface by p-polarized 800 nm, 150 fs laser pulses from a regeneratively amplified Ti:Sapphire laser (TSA-10, Spectra physics) running at 10 Hz, seeded by mode-locked pulses from a Ti:Sapphire oscillator (Tsunami, Spectra Physics). The linear optical transmission of the nanoparticle jets at 800 nm is adjusted to be about 75%, measured by using the unfocused laser beam at low energy. For the experiment the laser beam is focused to the jet using a plano-convex lens of 40 cm focal length, giving a focal spot size of 96 μm. The volume of liquid irradiated by each laser pulse is estimated to be 2.3×10^{-3} mL. The liquid flow rate is 16 ml/min (i.e., 26.7×10^{-3} ml per 100 m, which is the time interval between successive laser pulses). Therefore, every laser pulse irradiates a fresh sample of the liquid in the jet. The energy of the laser pulses is 5.5 mJ, which provides an intensity of $7.4 \times 10^{14}\,W/cm^2$ at the beam focus. X-rays are measured at a distance of 10 cm from the jet at an angle of 20° from the laser beam axis, which is the direction in which the emission is found to be maximum. A CdTe detector is used for the measurement, which has nearly 100% conversion efficiency in the energy range 10 KeV to 150 KeV. The energy of the incident photon determines the amplitude of the detector output.

The full sample volume will flow from the source beaker to the drain beaker in a time interval of 15 min (9000 laser pulses). A drop of the transferred solution is dried on an ITO sheet to form a film, which is used for taking the SEM image. The irradiated solution is then transferred from the drain beaker to the source beaker, and the process is repeated. Every 15 min (9000 pulses) is counted as one step of irradiation. In total nine steps of irradiation (81000 pulses, 135 min) were carried out.

3. Results and discussion

Fig. 3a shows the effect of laser irradiation on the linear absorption spectrum of Ag nanoparticles. The height of the LSPR band (which peaks at 410 nm) gets reduced indicating that the nanoparticle concentration is decreasing with laser irradiation. The concomitant rise of the long-wavelength wing is more obvious from Fig. 3b, in which the spectra are redrawn with all peak absorbances normalized to unity. The short-wavelength side also gets enhanced. This clearly indicates laser-induced aggregation of Ag nanoparticles [18]. Fig. 3c gives SEM images showing morphology changes.

Fig. 4a–c shows corresponding results obtained for Au nanoparticles. Here, the height of the LSPR band (which peaks at 520 nm) is noticeably reduced during the first step of irradiation itself, but thereafter the reduction is minimal. Broadening of the spectra with irradiation indicate agglomeration, but it is not as pronounced as in the case of Ag nanoparticles. This observation mean that Au nanoparticles are more photostable compared to Ag nanoparticles.

SEM images shown in Figs. 3c and 4c reveal morphology changes due to laser irradiation. For every laser pulse the nanoparticles will absorb a large number of photons, and their temperature will rise significantly, leading to fragmentation. The smaller nanoparticles produced by fragmentation might get further pulverized by multiphoton absorption [19]. The heat diffuses into the surrounding medium within picoseconds to nanoseconds, and the temperature of the nanoparticles is lowered, until the arrival of the following pulse. While the fragmentation process occurs for each laser pulse, the fragments will aggregate back into small clusters within nanoseconds, in the interim period between the pulses (at 10 Hz repetition rate the time interval between successive laser pulses is quite long at 100 m). The aggregation rate increases with the concentration of the fragments [19]. Notwithstanding the fact that Ag nanoparticles are less photostable compared to Au nanoparticles, it may be noted that the LSPR peak in Ag is in better resonance for two-photon absorption at the excitation wavelength of 800 nm compared to the LSPR peak of Au. Hence a larger number of Ag nanoparticles are likely to get fragmented and subsequently aggregated during each irradiation step. Broadening of the LSPR wing region indicates moderate aggregation leading to the formation of larger clusters [20].

Fig. 5 shows the energy spectrum of bremsstrahlung X-ray emission measured in the 15–100 keV region. Compared to Au nanoparticles,

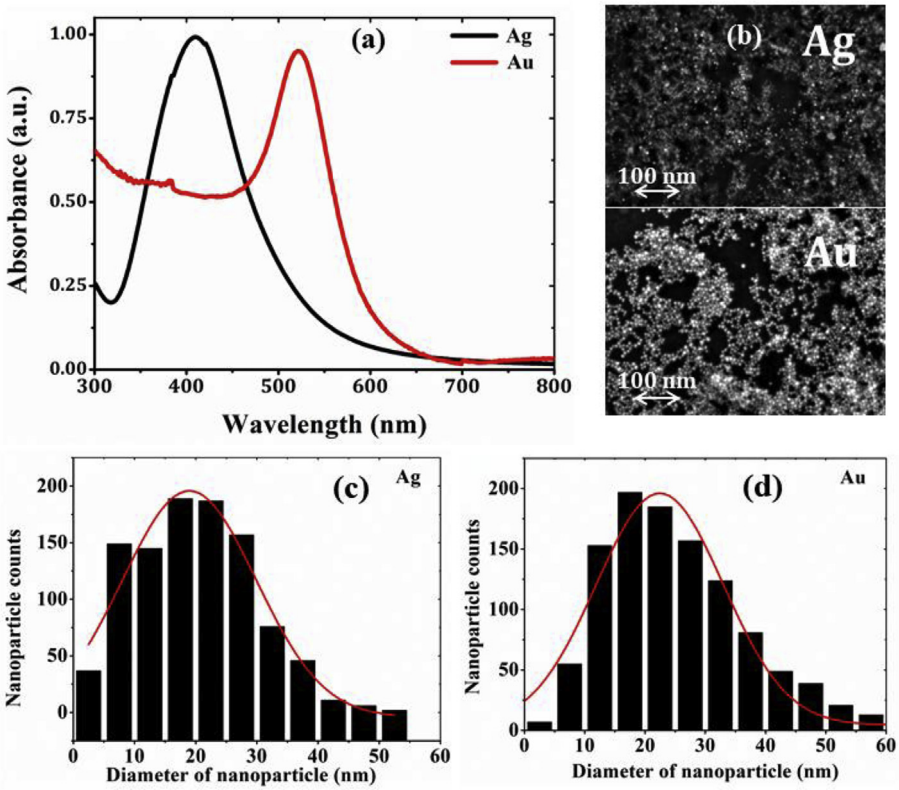

Fig. 1. (a) Absorption spectra of Ag and Au nanoparticle suspensions showing LSPR bands; (b) SEM images of as prepared Ag and Au nanoparticles; (c) & (d) size distribution histograms for Ag and Au nanoparticles calculated from SEM images.

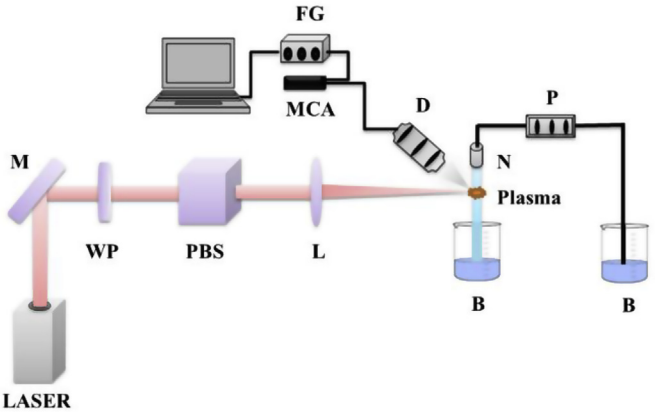

Fig. 2. Schematic of the experimental setup for bremsstrahlung X-ray generation. A thin (250 μm) jet of metal nanoparticles suspended in water is irradiated by 800 nm, 150 fs laser pulses. Pulse energy is 5.5 mJ and pulse repetition rate is 10 Hz. M-mirror, WP - half-wave plate, PBS – polarizing beam splitter, L – lens, B – beaker, N – thin metal nozzle, P – water pump, D – CdTe X-ray detector, FG – function generator, MCA – multi-channel analyzer.

peak X-ray emission is brighter by a factor of two for Ag nanoparticles. Similar measurements were carried out in DI water, and also in the precursor salt solutions: silver nitrate ($AgNO_3$), trisodium citrate and DI water for Ag nanoparticles, and hydrocholoroauric acid, citric acid and DI water for Au nanoparticles. Emission from the nanoparticle suspensions were found to be considerably higher compared to that from their precursor solutions, confirming that the nanoparticles are indeed responsible for the observed enhancement.

To explain these experimental results, first we note that the enhanced local electric field (E_1) associated with the LSPR is given by Ref. [21].

$$E_1 = \frac{3\in_d}{\in_m + 2\in_d} E_0 \tag{1}$$

where E_0 is the applied electric field (7.2×10^{10} V/m). $\in_m$ and $\in_d$ are the dielectric constants of the metal nanoparticle and the surrounding medium respectively, for 800 nm wavelength. The local electric fields calculated for Ag and Au nanoparticles are 1.22×10^{11} V/m and 1.16×10^{11} V/m respectively. The local field is thus one order of magnitude higher than the applied electric field, which causes a substantial increase in the MPI efficiency. Silver nanoparticles experience a slightly higher local field, generating relatively more number of hot electrons. Moreover, the ionization potentials of Ag and Au are 7.58 eV and 9.22 eV respectively, so that with 800 nm (1.55 eV) excitation, MPI of Ag is a 5-photon process while that of Au is a 6-photon process. Between these the 5-photon process will be relatively stronger, again resulting in a larger number of hot electrons for Ag.

Secondly, the photon energy (E) distribution of bremsstrahlung from hot electrons is given by Ref. [22].

$$N(E) \propto \frac{1}{T_e^{1/2}} \exp\left(-\frac{E}{kT_e}\right) \tag{2}$$

where T_e is the hot electron temperature and k is the Boltzmann constant. Therefore, T_e can be obtained by fitting this function to the measured energy-resolved bremsstrahlung spectrum. Since $T_e^{-\frac{1}{2}}$ is relatively slowly varying in comparison to the exponential term, a simple exponential fit to the experimental data is usually sufficient. The hot electron temperatures obtained for DI water, precursor salts of Ag nanoparticles ($AgNo_3$ + $Na_3C_6H_5O_7$ + DI water), and precursor salts of Au nanoparticles ($HAuCl_4$ + $C_6H_8O_7$ + DI water), are 4 ± 0.07 keV, 10 ± 0.04 keV, and 8 ± 0.06 keV, respectively (Fig. 5). Obviously, Ag and Au nanoparticles have higher electron temperatures compared to their precursors.

Finally, Fig. 6 depicts the scaling of hot electron temperature with

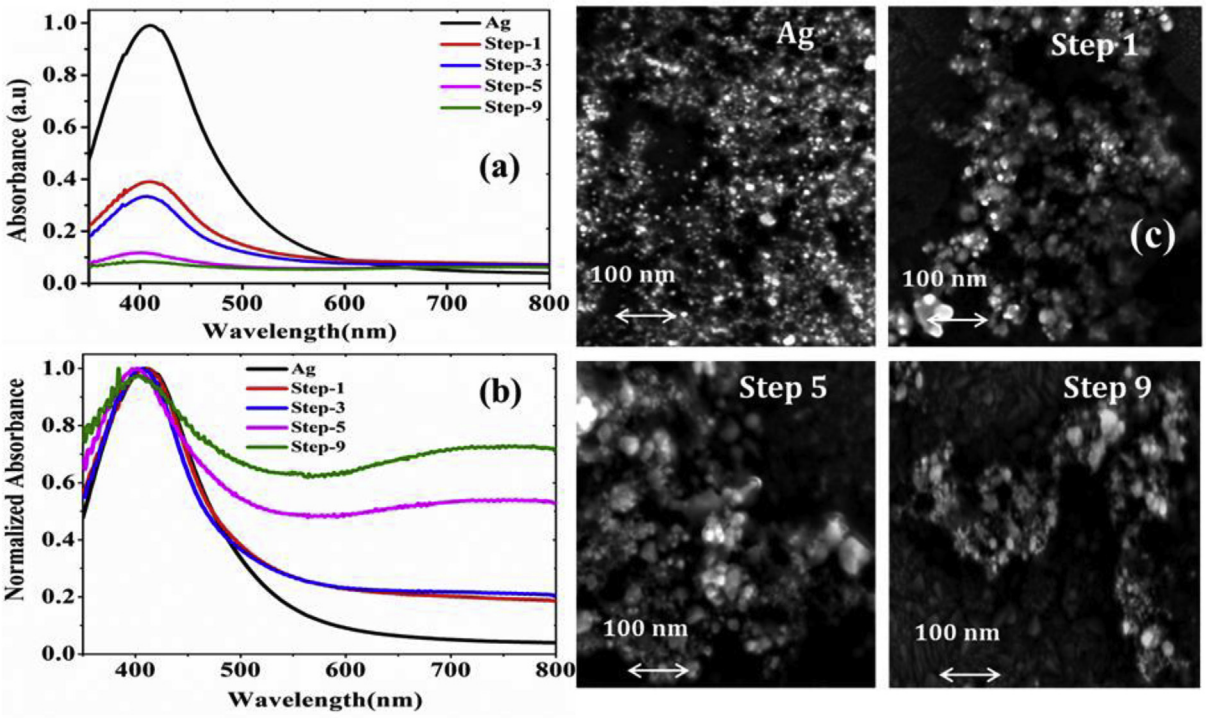

Fig. 3. (a) Linear absorption spectra of Ag nanoparticle suspension measured after successive steps of laser irradiation (each step is 9000 laser shots), (b) absorption spectra drawn with the peak absorbances normalized to unity, (c) SEM images showing morphology changes.

laser intensity, given by Refs. [23,24]

$$T_e \sim 14 T_c (I\lambda^2)^{\alpha} \quad (3)$$

where $I\lambda^2$ is the intensity in units of 10^{15} Wcm^{-2} μm^2 and T_c is the bulk plasma temperature (both T_c and T_e are given in keV). By taking T_c as 0.1 keV and substituting for the other quantities it turns out that $\alpha = 1/3$, which indicates that the hot electrons are generated by a resonance absorption mechanism [25]. In resonance absorption the p-polarized electromagnetic wave will resonantly excite electron oscillations in the plasma, the magnitude of which will grow until the oscillations are limited by collisional or collision-less damping processes. The longitudinal electric field component (E_z) plays a key role in electron heating leading to the generation of hot electrons, resulting in X-ray emission from the plasma [26,27].

4. Conclusion

We have measured bremsstrahlung X-ray emission from flowing thin jets of aqueous Ag and Au nanoparticle suspensions, excited by 800 nm laser pulses of 150 fs duration with intensities close to 10^{15} W/

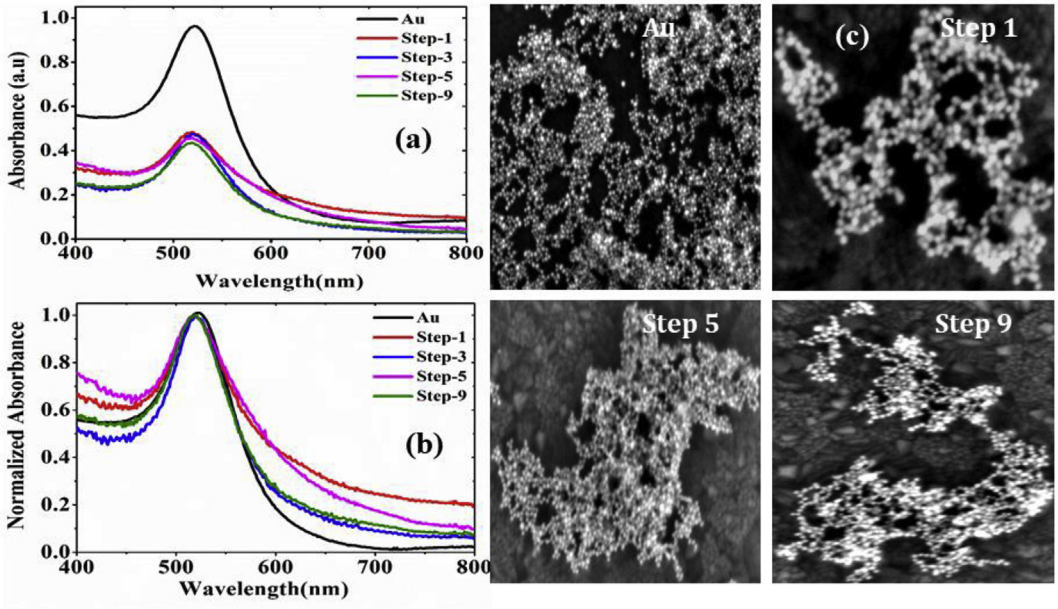

Fig. 4. (a) Absorption spectra of Au nanoparticle suspension measured after successive steps of laser irradiation (each step is 9000 laser shots), (b) absorption spectra drawn with the absorbances normalized to unity, (c) corresponding SEM images showing morphology changes.

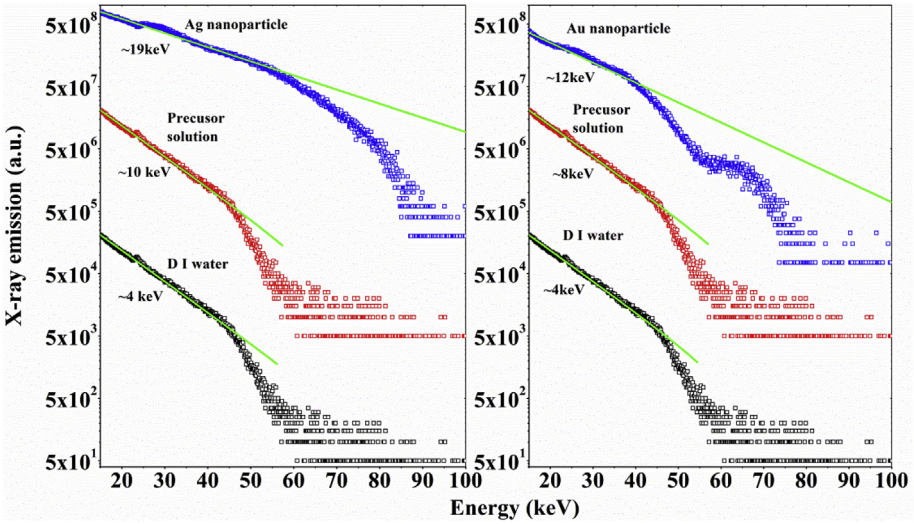

Fig. 5. Energy spectrum of bremsstrahlung X-ray emission measured in Ag and Au nanoparticle suspensions and their precursor solutions for a laser pulse intensity of 7.4×10^{14} W/cm^2. Total counts measured for the first 9000 laser pulses (step 1) are shown. Solid curves are numerical fits obtained using Equation (2).

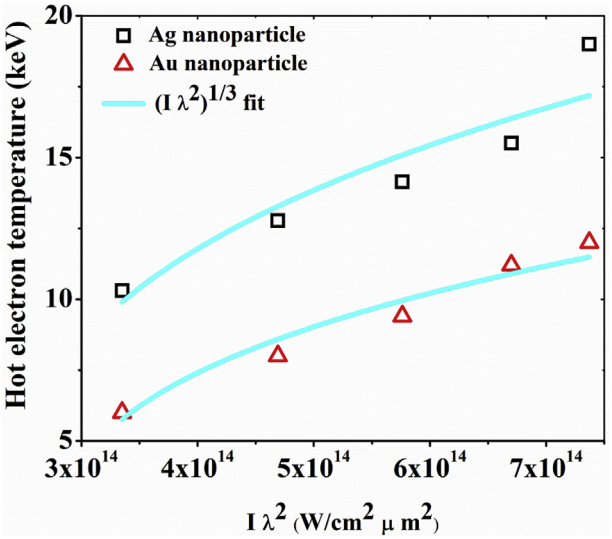

Fig. 6. Hot electron temperature versus $I\lambda^2$ for the generated plasmas. Solid curves are numerical fits to the data using Equation (3).

cm^2. When compared to the precursor salt solutions, 30-fold and 18-fold enhancements in X-ray yield have been observed for the Ag and Au nanocolloidal suspensions respectively. The relatively higher emission from Ag nanoparticles is attributed to the lower ionization potential and the higher local electric field, which are favorable for enhanced multiphoton ionization. While Ag nanoparticles exhibit a higher X-ray yield compared to Au nanoparticles, photostability is found to be better for the latter. These results show that liquid jets of noble metal nanoparticles are potential candidates for designing efficient and durable ultrafast laser plasma X-ray sources.

Acknowledgement

Authors thank Dr. Suchand Sandeep for technical discussions, and Ms. Vasudha and Mr. Yatheendran for absorption and SEM measurements respectively.

References

[1] R.C. Elton, X-ray Lasers, Academic Press, 1990.
[2] W. Chao, B.D. Harteneck, J.A. Liddle, E.H. Anderson, D.T. Attwood, Soft X-ray microscopy at a spatial resolution better than 15 nm, Nature 435 (2005) 1210–1213, https://doi.org/10.1038/nature03719.
[3] C. Rischel, A. Rousse, I. Uschmann, P.-A. Albouy, J.-P. Geindre, P. Audebert, J.-C. Gauthier, E. Froster, J.-L. Martin, A. Antonetti, Femtosecond time-resolved X-ray diffraction from laser-heated organic films, Nature 390 (1997) 490–492, https://doi.org/10.1038/37317.
[4] A.A. Oraevsky, L.B. Da Silva, A.M. Rubenchik, M.D. Feit, M.E. Glinsky, M.D. Perry, B.M. Mammini, W. Small, B.C. Stuart, Plasma mediated ablation of biological tissues with nanosecond-to-femtosecond laser pulses: relative role of linear and nonlinear absorption, IEEE J. Sel. Top. Quantum Electron. 2 (1996) 801–809, https://doi.org/10.1109/2944.577302.
[5] S. Fritzler, V. Malka, G. Grillon, J.P. Rousseau, F. Burgy, E. Lefebvre, E. D'Humières, P. McKenna, K.W.D. Ledingham, Proton beams generated with high-intensity lasers: applications to medical isotope production, Appl. Phys. Lett. 83 (2003) 3039–3041, https://doi.org/10.1063/1.1616661.
[6] A. Rousse, K. Ta Phuoc, R. Shah, A. Pukhov, E. Lefebvre, V. Malka, S. Kiselev, F. Burgy, J.P. Rousseau, D. Umstadter, D. Hulin, Production of a keV X-ray beam from synchrotron radiation in relativistic laser-plasma interaction, Phys. Rev. Lett. 93 (2004) 1–4, https://doi.org/10.1103/PhysRevLett.93.135005.
[7] L.M. Chen, M. Kando, M.H. Xu, Y.T. Li, J. Koga, M. Chen, H. Xu, X.H. Yuan, Q.L. Dong, Z.M. Sheng, S. V Bulanov, Y. Kato, J. Zhang, T. Tajima, Study of X-Ray Emission Enhancement via a High-Contrast Femtosecond Laser Interacting with a Solid Foil, (2008), pp. 1–4, https://doi.org/10.1103/PhysRevLett.100.045004 045004.
[8] K. Hatanaka, K. ichiro Yomogihata, H. Ono, K. Nagafuchi, H. Fukumura, M. Fukushima, T. Hashimoto, S. Juodkazis, H. Misawa, Hard X-ray generation using femtosecond irradiation of PbO glass, J. Non-Cryst. Solids 354 (2008) 5485–5490, https://doi.org/10.1016/j.jnoncrysol.2008.09.013.
[9] T. Nishikawa, H. Nakano, K. Oguri, N. Uesugi, M. Nakao, K. Nishio, H. Masuda, Nanocylinder-array structure greatly increases the soft X-ray intensity generated from femtosecond laser-produced plasma, Appl. Phys. B Laser Opt. 73 (2001) 185–188, https://doi.org/10.1007/s003400100625.
[10] M.M. Murnane, H.C. Kapteyn, S.P. Gordon, J. Bokor, E.N. Glytsis, R.W. Falcone, Efficient coupling of high-intensity subpicosecond laser pulses into solids, Appl. Phys. Lett. 62 (1993) 1068–1070, https://doi.org/10.1063/1.108797.
[11] S.P. Gordon, T. Donnelly, a Sullivan, H. Hamster, R.W. Falcone, X rays from microstructured targets heated by femtosecond lasers, Opt. Lett. 19 (1994) 484–486, https://doi.org/10.1364/OL.19.000484.
[12] G. Kulcsár, D. Al Mawlawi, F.W. Budnik, P.R. Herman, M. Moskovits, L. Zhao, R.S. Marjoribanks, Intense picosecond x-ray pulses from laser plasmas by use of nanostructured "velvet" targets, Phys. Rev. Lett. 84 (2000) 5149–5152, https://doi.org/10.1103/PhysRevLett.84.5149.
[13] S. Bagchi, P.P. Kiran, K. Yang, A.M. Rao, M.K. Bhuyan, M. Krishnamurthy, G.R. Kumar, Bright, low debris, ultrashort hard x-ray table top source using carbon nanotubes, Phys. Plasmas 18 (2011) 0–4, https://doi.org/10.1063/1.3531685.
[14] F.C.P. Masim, M. Porta, W.H. Hsu, M.T. Nguyen, T. Yonezawa, A. Balčytis, S. Juodkazis, K. Hatanaka, Au nanoplasma as efficient hard X-ray emission source, ACS Photonics 3 (2016) 2184–2190, https://doi.org/10.1021/acsphotonics.6b00692.
[15] P.P. Rajeev, P. Taneja, P. Ayyub, A.S. Sandhu, G.R. Kumar, Metal Nanoplasmas as Bright Sources of Hard X-Ray Pulses, (2003), pp. 11–14, https://doi.org/10.1103/PhysRevLett.90.115002.
[16] S. Mondal, I. Chakraborty, S. Ahmad, D. Carvalho, P. Singh, A.D. Lad, V. Narayanan, P. Ayyub, G.R. Kumar, Highly Enhanced Hard X-Ray Emission from Oriented Metal Nanorod Arrays Excited by Intense Femtosecond Laser Pulses,

(2011), pp. 1–5, https://doi.org/10.1103/PhysRevB.83.035408 035408.
[17] A. Zielińska, E. Skwarek, A. Zaleska, M. Gazda, J. Hupka, Preparation of silver nanoparticles with controlled particle size, Procedia Chem. 1 (2009) 1560–1566, https://doi.org/10.1016/j.proche.2009.11.004.
[18] J. Turkevich, Colloidal gold. Part I, Gold Bull. 18 (1985) 86–91, https://doi.org/10.1007/BF03214690.
[19] F. Mafune, J. Kohno, Y. Takeda, T. Kondow, Dissociation and Aggregation of Gold Nanoparticles under Laser Irradiation, (2001), pp. 9050–9056.
[20] S. Link, Z.L. Wang, M.A. El-Sayed, Alloy formation of Gold − Silver nanoparticles and the dependence of the plasmon absorption on their composition, J. Phys. Chem. B 103 (1999) 3529–3533, https://doi.org/10.1021/jp990387w.
[21] A. Reza, A.S.M. Noor, M. Maarof, Application of surface plasmon resonance based on a metal nanoparticle, Plasmon. - Princ. Appl., InTech, 2012, https://doi.org/10.5772/51219.
[22] P.P. Rajeev, P. Ayyub, S. Bagchi, G.R. Kumar, Nanostructures, local fields, and enhanced absorption in intense light–matter interaction, Opt. Lett. 29 (2004) 2662, https://doi.org/10.1364/OL.29.002662.
[23] D.W. Forslund, J.M. Kindel, K. Lee, Theory of hot-electron spectra at high laser intensity, Phys. Rev. Lett. 39 (1977) 284–288, https://doi.org/10.1103/PhysRevLett.39.284.
[24] M. Anand, P. Gibbon, M. Krishnamurthy, Hot electrons produced from long scale-length laser-produced droplet plasmas, Laser Phys. 17 (2007) 408–414, https://doi.org/10.1134/S1054660X07040160.
[25] Y.-Q. Cui, W.-M. Wang, Z.-M. Sheng, Y.-T. Li, J. Zhang, Laser absorption and hot electron temperature scalings in laser–plasma interactions, Plasma Phys. Contr. Fusion 55 (2013) 085008, , https://doi.org/10.1088/0741-3335/55/8/085008.
[26] J.P. Palastro, J.G. Shaw, R.K. Follett, A. Colaïtis, D. Turnbull, A.V. Maximov, V.N. Goncharov, D.H. Froula, Resonance absorption of a broadband laser pulse, Phys. Plasmas 25 (2018), https://doi.org/10.1063/1.5063589 123104.
[27] W.-H. Hsu, F.C.P. Masim, M. Porta, M.T. Nguyen, T. Yonezawa, A. Balčytis, X. Wang, L. Rosa, S. Juodkazis, K. Hatanaka, Femtosecond laser-induced hard X-ray generation in air from a solution flow of Au nano-sphere suspension using an automatic positioning system, Optic Express 24 (2016) 19994, https://doi.org/10.1364/OE.24.019994.